J|A|C|S
ARTICLES

Published on Web 01/13/2010

# Interaction of Molecular Hydrogen with Microporous Metal Organic Framework Materials at Room Temperature

Nour Nijem,[†] Jean-François Veyan,[†] Lingzhu Kong,[‡] Kunhao Li,[§] Sanhita Pramanik,[§] Yonggang Zhao,[§] Jing Li,[§] David Langreth,[‡] and Yves J. Chabal*[,†]

*Department of Materials Science & Engineering, University of Texas at Dallas, Richardson, Texas 75080, and Department of Physics and Astronomy and Department of Chemistry and Chemical Biology, Rutgers University, 610 Taylor Road, Piscataway, New Jersey 08854*

Received October 15, 2009; E-mail: chabal@utdallas.edu

***Abstract:*** Infrared (IR) absorption spectroscopy measurements, performed at 300 K and high pressures (27−55 bar) on several prototypes of metal organic framework (MOF) materials, reveal that the MOF ligands are weakly perturbed upon incorporation of guest molecules and that the molecular hydrogen ($H_2$) stretch mode is red-shifted (30−40 $cm^{-1}$) from its unperturbed value (4155 $cm^{-1}$ for ortho $H_2$). For MOFs of the form M(bdc)(ted)$_{0.5}$ (bdc = 1,4-benzenedicarboxylate; ted = triethylenediamine), $H_2$ molecules interact with the organic ligands instead of the saturated metal centers located at the corners of the unit cell. First-principles van der Waals density functional calculations identify the binding sites and further show that the induced dipole associated with the trapped $H_2$ depends sensitively on these sites. For M(bdc)(ted)$_{0.5}$ systems, the strongest dipole moment is of the site that is in the corner of the unit cell and is dominated by the interaction with the benzene ligand and not by the metal center. For MOFs of the $M_3[HCOO]_6$ type with relatively short ligands (i.e., formate) and 1-D pore structures, there is a weak dependence of $H_2$ vibrational frequency on the cations, due to a small change in the unit cell dimension. Furthermore, translational states of $\sim\pm100$ $cm^{-1}$ are clearly observed as side bands on the $H_2$ stretch mode in these 1-D channels interconnected by very small apertures. The $H_2$ stretch IR integrated areas in all the MOFs considered in this work increase linearly with $H_2$ pressure, consistent with isotherm measurements performed in similar conditions. However, the IR intensity varies substantially, depending on the number of benzene rings interacting with the $H_2$ molecules. Finally, there is no correlation between $H_2$ binding energies (determined by isotherm measurements) and the magnitude of the $H_2$ stretch shift, indicating that IR shifts are dominated by the environment (organic ligand, metal center, and structure) rather than the strength of the interaction. These results highlight the relevance of IR spectroscopy to determine the type and arrangement of ligands in the structure of MOFs.

## 1. Introduction

Hydrogen is attractive for energy storage because it is abundant in water and is a pollution-free fuel with a clean reaction product (water). It has an exceptional mass energy density but, unfortunately, a low volume energy density, making it difficult to store at standard temperatures and pressures. Several ways of storing hydrogen in materials have been developed, either by chemical incorporation into materials such as complex metal hydrides or by weak adsorption into microporous material such as zeolites, carbon materials, and metal organic frameworks (MOFs).[1−8] On-board (i.e., transportation) applications require materials that can store and deliver hydrogen at reasonable temperatures (∼300 K) and pressures (<50 bar). Microporous MOF materials could be promising candidates for hydrogen storage since their high surface area and porosity make it possible to utilize physisorption as a storage strategy to store and deliver hydrogen at reasonable pressures and cryogenic temperatures.[6,9−17] Indeed, MOFs are composed of metal or metal oxide vertices that are connected via organic ligands forming porous structures that are readily accessible by $H_2$ molecules. Different MOF systems have been developed over the past 10 years since their discovery by Yaghi et al. in 1999.[7,18−24] Many of the studies have shown that MOFs can be easily tailored by changing the organic linkers and/or metal centers to generate different structures with controllable pore

[†] University of Texas at Dallas.
[‡] Department of Physics and Astronomy, Rutgers University.
[§] Department of Chemistry and Chemical Biology, Rutgers University.

(1) Murray, L. J.; Dinca, M.; Long, J. R. *Chem. Soc. Rev.* **2009**, *38*, 1294–1314.
(2) Zhao, X. Y.; Ma, L. Q. *Int. J. Hydrogen Energy* **2009**, *34*, 4788–4796.
(3) Zhao, X. B.; Xiao, B.; Fletcher, A. J.; Thomas, K. M. *J. Phys. Chem. B* **2005**, *109*, 8880–8888.
(4) Rangel, C. M.; Fernandes, V. R.; Slavkou, Y.; Bozukov, L. *Int. J. Hydrogen Energy* **2009**, *34*, 4587–4591.
(5) Silvestre-Albero, A. M.; Wahby, A.; Silvestre-Albero, J.; Rodriguez-Reinoso, F.; Betz, W. *Ind. Eng. Chem. Res.* **2009**, *48*, 7125–7131.
(6) Lan, A. J. *Inorg. Chem.* **2009**, *48*, 7165–7173.
(7) Xue, M.; Liu, Y.; Schaffino, R. M.; Xiang, S. C.; Zhao, X. J.; Zhu, G. S.; Qiu, S. L.; Chen, B. L. *Inorg. Chem.* **2009**, *48*, 4649–4651.
(8) Yu, X. B.; Guo, Y. H.; Yang, Z. X.; Guo, Z. P.; Liu, H. K.; Dou, S. X. *Scr. Mater.* **2009**, *61*, 469–472.

 **10.1021/ja908817n** 

size and shape.[25−27] Consequently, MOF systems are being considered for a variety of potential applications, including gas separation and storage, catalysis, and sensing.[23,28,29] The major drawback of such systems for hydrogen storage applications, however, is the weak $H_2$ binding energies that have currently achieved ∼7−10 kJ/mol, i.e., well below the 20−25 kJ/mol of $H_2$ required for on-board applications.[30]

Increasing $H_2$ binding energies in MOFs has been the focal point of numerous studies. Many groups are synthesizing and examining unsaturated metal center MOFs.[31−36] MOFs with *unsaturated* metal centers have shown an enhanced hydrogen uptake and higher binding energies due to the strong metal adsorption sites. In contrast, $H_2$ interaction in MOFs with *saturated* metal centers is often dominated by the organic ligands because the metal centers are fully coordinated. Since MOFs with saturated metal centers are usually more chemically stable, it is important to understand the role of the different organic linkers and the potential influence of the metal cations on $H_2$ incorporation in such MOF systems. In the present work we therefore examine MOFs with different types of ligands and metal centers leading to different structures. Aromatic and aliphatic ligands are used to construct 3-D metal organic frameworks with 3-D and 1-D pore structures. The goal of this study is to understand the influence of organic ligands on $H_2$ interaction and the role of the metal center on the ligand's environment for the different pore structures. Such understanding will help a more rational design of MOFs to meet the hydrogen uptake requirements.

Isotherm adsorption measurements give valuable information about hydrogen uptake and effective binding energies of $H_2$ in MOFs. However, they do not provide specific information about hydrogen adsorption sites and interaction strengths. Infrared (IR) absorption measurements on the other hand have the advantage of being sensitive to interaction potentials and specific adsorption sites within the host and have been used to study $H_2$ incorporation in solids.[37−41] Room temperature IR investigations of $H_2$ interaction with MOFs are difficult because $H_2$ uptake is usually small (<1 wt %) even at high pressures (∼50 bar). Therefore, to characterize such weak interactions at ambient temperatures, in situ IR measurements need to be implemented with high-pressure capabilities to probe specific site interactions within the different MOF systems. Since the H−H stretching of free $H_2$ molecules is IR inactive, IR spectroscopy is only sensitive to $H_2$ molecules that are interacting with a host (or other molecules), i.e., that undergo a perturbation of the local H−H symmetry. This perturbation is usually accompanied by a red shift of the H−H stretching modes, located at 4161.1 and 4155 $cm^{-1}$ for para and ortho $H_2$, respectively.[42]

To date, IR absorption studies of $H_2$ in MOF systems have been restricted to low temperatures and pressures.[37,38] At reasonable pressures (∼1 bar), MOF loading is much higher at low temperatures (77 K) than room temperature, and the spectral features are sharper, facilitating the detection of the weak induced absorption of $H_2$. However, a number of effects can take place at low temperatures, including water condensation (on system windows or competition into MOF adsorption sites) and changes in MOF structures, making it harder to decouple the hydrogen interaction from other structural effects. Moreover, practical hydrogen storage applications require the ability to store and release hydrogen at room temperature, and thus, the investigation of MOF−$H_2$ interactions under ambient conditions is essential for further developments in this field.

In the present study, we have characterized the interaction of the hydrogen at room temperature and high pressures (27−55 bar) using IR spectroscopy and isotherm measurements with four different types of microporous MOF compounds, varying the organic ligand, metal center, and structure (see Figure S1 in the Supporting Information). The first group of compounds has the general formula $M(bdc)(ted)_{0.5}$ (M = Zn, Ni, Cu; bdc = 1,4-benzenedicarboxylate; ted = triethylenediamine). For all three metals, the compounds are isostructural and crystallize in the tetragonal crystal system (space group *P*4/*ncc*). The


(9) Wong-Foy, A. G.; Matzger, A. J.; Yaghi, O. M. *J. Am. Chem. Soc.* **2006**, *128*, 3494–3495.
(10) Furukawa, H.; Miller, M. A.; Yaghi, O. M. *J. Mater. Chem.* **2007**, *17*, 3197–3204.
(11) Chen, B. L.; Ockwig, N. W.; Millward, A. R.; Contreras, D. S.; Yaghi, O. M. *Angew. Chem., Int. Ed.* **2005**, *44*, 4745–4749.
(12) Rowsell, J. L. C.; Millward, A. R.; Mueller, U.; Yaghi, O. M. *Abstr. Pap.−Am. Chem. Soc.* **2004**, *227*, 390-INOR.
(13) Rowsell, J. L. C.; Yaghi, O. M. *Angew. Chem., Int. Ed.* **2005**, *44*, 4670–4679.
(14) Rosi, N. L.; Eckert, J.; Eddaoudi, M.; Vodak, D. T.; Kim, J.; O'Keeffe, M.; Yaghi, O. M. *Science* **2003**, *300*, 1127–1129.
(15) Zhao, D.; Yuan, D. Q.; Zhou, H. C. *Energy Environ. Sci.* **2008**, *1*, 222–235.
(16) Liu, J.; Lee, J. Y.; Pan, L.; Obermyer, R. T.; Simizu, S.; Zande, B.; Li, J.; Sankar, S. G.; Johnson, J. K. *J. Phys. Chem. C* **2008**, *112*, 2911–2917.
(17) Thomas, K. M. *Dalton Trans.* **2009**, 1487–1505.
(18) Li, H.; Eddaoudi, M.; O'Keeffe, M.; Yaghi, O. M. *Nature* **1999**, *402*, 276–279.
(19) Sudik, A. C.; Millward, A. R.; Ockwig, N. W.; Cote, A. P.; Kim, J.; Yaghi, O. M. *J. Am. Chem. Soc.* **2005**, *127*, 7110–7118.
(20) Yaghi, O. M.; O'Keeffe, M.; Ockwig, N. W.; Chae, H. K.; Eddaoudi, M.; Kim, J. *Nature* **2003**, *423*, 705–714.
(21) Tranchemontagne, D. J.; Hunt, J. R.; Yaghi, O. M. *Tetrahedron* **2008**, *64*, 8553–8557.
(22) Xu, J.; Bai, Z. S.; Okamura, T. A.; Chen, M. S.; Sun, W. Y.; Ueyama, N. *Polyhedron* **2009**, *28*, 2480–2486.
(23) Dai, F. N.; He, H. Y.; Gao, D. L.; Ye, F.; Sun, D. F.; Pang, Z. J.; Zhang, L.; Dong, G. L.; Zhang, C. Q. *Inorg. Chim. Acta* **2009**, *362*, 3987–3992.
(24) Nouar, F.; Eckert, J.; Eubank, J. F.; Forster, P.; Eddaoudi, M. *J. Am. Chem. Soc.* **2009**, *131*, 2864–2870.
(25) Eddaoudi, M.; Kim, J.; Rosi, N.; Vodak, D.; Wachter, J.; O'Keeffe, M.; Yaghi, O. M. *Science* **2002**, *295*, 469–472.
(26) Chae, H. K.; Kim, J.; Friedrichs, O. D.; O'Keefe, M.; Yaghi, O. M. *Angew. Chem., Int. Ed.* **2003**, *42*, 3907–3909.
(27) Rosi, N. L.; Eddaoudi, M.; Kim, J.; O'Keeffe, M.; Yaghi, O. M. *CrystEngComm* **2002**, 401–404.
(28) Bae, Y. S.; Farha, O. K.; Hupp, J. T.; Snurr, R. Q. *J. Mater. Chem.* **2009**, *19*, 2131–2134.
(29) Kuppler, R. J.; Timmons, D. J.; Fang, Q.-R.; Li, J.-R.; Makal, T. A.; Young, M. D.; Yuan, D.; Zhao, D.; Zhuang, W.; Zhou, H.-C. *Coord. Chem. Rev.* **2009**, *253*, 3042–3066.
(30) Satyapal, S.; Petrovic, J.; Read, C.; Thomas, G.; Ordaz, G. *Catal. Today* **2007**, *120*, 246–256.
(31) Niu, J.; Rao, B. K.; Jena, P. *Phys. Rev. Lett.* **1992**, *68*, 2277.
(32) Kubas, G. J. *Acc. Chem. Res.* **1988**, *21*, 120–128.
(33) Zhou, W.; Wu, H.; Yildirim, T. *J. Am. Chem. Soc.* **2008**, *130*, 15268–15269.
(34) Zhou, W.; Yildirim, T. *J. Phys. Chem. C* **2008**, *112*, 8132–8135.
(35) Wu, H.; Zhou, W.; Yildirim, T. *J. Am. Chem. Soc.* **2009**, *131*, 4995–5000.
(36) Liu, Y.; Kabbour, H.; Brown, C. M.; Neumann, D. A.; Ahn, C. C. *Langmuir* **2008**, *24*, 4772–4777.
(37) Bordiga, S.; Vitillo, J. G.; Ricchiardi, G.; Regli, L.; Cocina, D.; Zecchina, A.; Arstad, B.; Bjørgen, M.; Hafizovic, J.; Lillerud, K. P. *J. Phys. Chem. B* **2005**, *109*, 18237–18242.
(38) Vitillo, J. G.; Regli, L.; Chavan, S.; Ricchiardi, G.; Spoto, G.; Dietzel, P. D. C.; Bordiga, S.; Zecchina, A. *J. Am. Chem. Soc.* **2008**, *130*, 8386–8396.
(39) Chabal, Y. J.; Patel, C. K. N. *Rev. Mod. Phys.* **1987**, *59*, 835–844.
(40) Chaudhuri, S.; Rangan, S.; Veyan, J. F.; Muckerman, J. T.; Chabal, Y. J. *J. Am. Chem. Soc.* **2008**, *130*, 10576–10587.
(41) Gribov, E. N.; Cocina, D.; Spoto, G.; Bordiga, S.; Ricchiardi, G.; Zecchina, A. *Phys. Chem. Chem. Phys.* **2006**, *8*, 1186–1196.
(42) Welsh, H. L. *J. Atmos. Sci.* **1969**, *26*, 835.

framework is composed of a paddle-wheel $M_2(COO)_4$ secondary building unit (SBU) that is interconnected via bdc and ted, giving rise to a 3-D pore structure with relatively large pore size (~7−8 Å), pore volume (~0.63−0.84 $cm^3/g$), and BET surface area (~1500−1900 $m^2/g$).[43] The second group of compounds investigated has crystal and pore structures similar to those of $M(bdc)(ted)_{0.5}$, but the ligands are aliphatic rather than aromatic. The general molecular formula is $M(bodc)(ted)_{0.5}$ (M = Ni, Co; bodc = bicyclo[2.2.2]octane-1,4-dicarboxylate).[44] The third group of compounds has the general formula $M_3(HCOO)_6$ (M = Ni, Mn, Co; HCOO = formate or fa) made of an $M_5$ SBU. The structures crystallize in space group $P2_1/c$ and feature 1-D open channels with smaller pore diameters (~5−6 Å).[45,46] The fourth group is a more complex 3-D structure with 1-D pores, $Zn_2(bpdc)_2(bpee)$, where bpdc = 4,4′-biphenyldicarboxylate and bpee = 1,2-bipyridylethene, made of layers of 2-fold interpenetrating Zn(bpdc) nets interconnected by bpee ligands.[47] The SBU in this structure is an $M_2(bpdc)_4$ unit.

In this work we investigate hydrogen interaction in MOFs uniquely combining infrared spectroscopy at room temperature with a van der Waals density functional (vdW-DF) method. The theoretical approach incorporates van der Waals interactions into a fully nonlocal and nonempirical density functional for the correlation energy while retaining the ordinary density functional theory's good description of covalent bonding.[48−50] It is particularly useful in locating the binding sites and understanding the MOF−$H_2$ interaction. In the present study, using a new algorithm,[51] we are able to perform self-consistent calculations for these MOF−$H_2$ systems and relax the adsorbed $H_2$ in the search of the strongest binding position and orientation. The stretching mode frequencies can then be calculated by a series of total energy calculations with different H−H bond lengths at equilibrium positions, yielding results that are consistent with IR data. Furthermore, the detailed energy landscape near equilibrium allows us to extract the dynamical properties of the adsorbed dihydrogen such as the translational movement and hindered rotation, thus obtaining a picture for the translational movements of the $H_2$ molecules that is consistent with the experimental findings. The self-consistent vdw-DF charge density also permits the calculation of induced dipole moments (i.e., IR intensities) for adsorbed $H_2$ when the interaction between adjacent cells can be neglected. We find for instance that one of the adsorption sites in $Zn(bdc)(ted)_{0.5}$ has a dipole moment about 2 orders of magnitude smaller than the other one and therefore has negligible contribution to the IR spectrum. These computational results in conjunction with the IR spectra shed further light on the MOF−$H_2$ interactions in these systems.

## 2. Materials and Methods

**2.1. Material Synthesis. 2.1.1. $Zn(bdc)(ted)_{0.5}$.** Synthesis was performed by heating a mixture of zinc(II) nitrate hexahydrate (0.380 g), terepthalic acid ($H_2bdc$; 0.252 g), and ted (0.137 g) in DMF (10 mL, with 2 drops of concentrated nitric acid added) at 120 °C for 4 days, yielding a colorless crystalline powder.

**2.1.2. $Ni(bdc)(ted)_{0.5}$.** Synthesis was performed by heating a mixture of nickel(II) nitrate hexahydrate (0.375 g), $H_2bdc$ (0.247 g), and ted (0.135 g) in DMF (10 mL, with 2 drops of concentrated nitric acid added) at 120 °C for 4 days, yielding a green crystalline powder.

**2.1.3. $Cu(bdc)(ted)_{0.5}$.** Synthesis was performed by heating a mixture of copper nitrate trihydrate (0.740 g), $H_2bdc$ (0.680 g), and ted (0.480 g) in 150 mL of DMF at 120 °C for 1.5 days, yielding a blue-colored crystalline powder of $Cu(bdc)(ted)_{0.5}$ (0.85 g).

**2.1.4. $Mn_3(HCOO)_6$.** Synthesis was performed by heating a mixture of manganese(II) acetate tetrahydrate (0.600 g, 2.4 mmol) and formic acid (2 mL, 97%, 51.4 mmol) in DMF (30 mL) in an oven at 100 °C for 48 h. The slightly pink crystalline precipitate was filtered, rinsed with DMF (10 mL) and diethyl ether (10 mL), and dried under vacuum for 5 min (0.350 g obtained, 86% yield based on manganese nitrate).

**2.1.5. $Ni_3(HCOO)_6$.** Synthesis was performed by heating a mixture of nickel(II) nitrate hexahydrate (1.142 g) and formic acid (1.0 mL) in DMF (8 mL) at 100 °C for 13 h, yielding a light green crystalline powder (0.590 g). The same filtering and isolation procedure as for $Mn_3(HCOO)_6$ was used as well.

**2.1.6. $Zn_2(bpdc)_2(bpee)$.** A mixture of $Zn(NO_3)_2 \cdot 6H_2O$ (0.0896 g, 0.30 mmol), $H_2bpdc$ (0.0720 g, 0.30 mmol), and bpee (0.0547 g, 0.30 mmol) in DMF (12 mL) was heated at 165 °C for 3 days to give 0.100 g of colorless microcrystals.

**2.2. Methods: Activation Procedure.** When synthesized, the majority of the MOF pores are occluded with the organic solvent used in the synthesis, in our case dimethyleformamide (DMF). In general, organic molecules can be removed from the pores by two main methods, either heating under reduced pressures or performing a solvent exchange.[52] Heating was performed at 120 °C under reduced pressure ($10^{-4}$ Torr) (Figure S2 in the Supporting Information shows the disappearance of the IR band at 1678 $cm^{-1}$ corresponding to $\nu$(C═O) in the DMF due to heating in a vacuum). Chemical exchange involved immersion in chloroform solvent for a few days followed by an overnight drying cycle in reduced pressure. Recent studies have shown that the surface area resulting from the solvent exchange method is much larger than that resulting from heating.[53] The two methods were tested for each sample, and the procedure that gave the largest $H_2$ loading and most reliable results was selected.

**2.3. IR Spectroscopy of $H_2$ Adsorption.** Infrared absorption spectroscopy measurements were done in transmission at room temperature using a liquid $N_2$ cooled indium antimonide detector for the near-IR region (4000−5000 $cm^{-1}$) and a liquid $N_2$ cooled MCT/A for the mid-IR region (650−4000 $cm^{-1}$). A portion of the activated MOF powder (~10 mg for the near-IR measurements and ~2 mg for the mid-IR measurements) was lightly pressed onto a KBr support, mounted into a high-temperature, high pressure cell (Specac product number P/N 5850c), and further heated in a vacuum. Hydrogen pressures of 27−55 bar were introduced into the cell, using deuterium gas as a reference for the hydrogen absorption spectra, as explained in the next section.

In these working pressure conditions, collision-induced IR absorption is easily detectable and must be removed from the final absorption spectra.[42] Indeed, homonuclear diatomic molecules such as hydrogen have a center of symmetry and therefore are IR inactive. However, in a pressurized gas the distortion of the electron

(43) Lee, J. Y.; Olson, D. H.; Pan, L.; Emge, T. J.; Li, J. *Adv. Funct. Mater.* **2007**, *17*, 1255–1262.
(44) Li, K.; Lee, J.; Olson, D. H.; Emge, T. J.; Bi, W.; Eibling, M. J.; Li, J. *Chem. Commun.* **2008**, 6123–6125.
(45) Kunhao, L.; David, H. O.; Jeong Yong, L.; Wenhua, B.; Ke, W.; Tan, Y.; Qiang, X.; Li, J. *Adv. Funct. Mater.* **2008**, *18*, 2205–2214.
(46) Wang, Z.; Zhang, B.; Zhang, Y.; Kurmoo, M.; Liu, T.; Gao, S.; Kobayashi, H. *Polyhedron* **2007**, *26*, 2207–2215.
(47) Anjian, L.; Kunhao, L.; Haohan, W.; David, H. O.; Thomas, J. E.; Woosoek, K.; Maochun, H.; Jing, L. *Angew. Chem., Int. Ed.* **2009**, *48*, 2334–2338.
(48) Dion, M.; Rydberg, H.; Schröder, E.; Langreth, D. C.; Lundqvist, B. I. *Phys. Rev. Lett.* **2004**, *92*, 246401.
(49) Dion, M.; Rydberg, H.; Schröder, E.; Langreth, D. C.; Lundqvist, B. I. *Phys. Rev. Lett.* **2005**, *95*, 109902.
(50) Thonhauser, T.; Valentino, R. C.; Shen, L.; Aaron, P.; Per, H.; David, C. L. *Phys. Rev. B: Condens. Matter* **2007**, *76*, 125112.
(51) Roman-Perez, G.; Soler, J. M. *Phys. Rev. Lett.* **2009**, *103*, 096102.
(52) Li, J.; Cheng, S.; Zhao, Q.; Long, P.; Dong, J. *Int. J. Hydrogen Energy* **2009**, *34*, 1377–1382.
(53) Nelson, A. P.; Farha, O. K.; Mulfort, K. L.; Hupp, J. T. *J. Am. Chem. Soc.* **2009**, *131*, 458-+.

distribution due to binary and higher order collisions induces a dipole moment resulting in IR absorption.[42] Therefore, hydrogen gas references needed to be taken at each pressure and subtracted from the absorption spectra of the MOF as shown in Figure S3 in the Supporting Information.

**2.4. Theoretical Methods.** First-principles calculations based on van der Waals density functional theory were performed within the plane-wave implementation of the density functional theory in the ABINIT[54,55] package, which we have adapted from the Siesta[56,57] code to incorporate the van der Waals interaction. We used Troullier−Martins pseudopotentials[58] with a gradient-corrected functional. An energy cutoff of 50 Ry and $\gamma$ point sampling were found to be enough to converge the interaction energy within 0.1 kJ/mol and the frequency shift within 1 $cm^{-1}$. We performed calculations for the systems of $Zn(bdc)(ted)_{0.5}$, $Cu(bdc)(ted)_{0.5}$, and $Zn(bpdc)_2(bpee)$. For $Zn(bdc)(ted)_{0.5}$ we used the experimentally derived structure, while for $Cu(bdc)(ted)_{0.5}$, which has no single-crystal experimental data, we relaxed the structure using the $Zn(bdc)(ted)_{0.5}$ data as input. For $Zn_2(bpdc)_2(bpee)$, the structure used in the calculations was determined by removal of the guest molecules, followed by relaxing that structure.

To calculate the vibrational frequency, we first preformed a series of total energy calculations with different $H_2$ bond lengths while keeping the center of $H_2$ and the MOF atoms at their equilibrium positions. The resulting total energies were used in the Schrodinger equation to obtain the eigenvalues, and the difference of the two lowest eigenlevels gives the vibrational frequency.

The dipole moment is estimated from $\mu = -e \int r(\rho^{MOF+H_2} - \rho^{MOF})\, dr$, where $e$ is the electron charge and $\rho^{MOF+H_2}$ is the total charge density of the MOF/$H_2$ system while $\rho^{MOF}$ is that of the pure MOF. The integral boundaries have to be large enough to converge the dipole calculation. However, a supercell calculation with no $H_2$ in neighboring cells would be too large to be tractable for unit cells in MOFs. We carried out the integral over the unit cell where it was not fully converged due to interactions from $H_2$ in neighboring cells. The moment calculated from this integral only gives a rough approximation to the true value. However, the large difference between the dipoles of $H_2$ at different positions in the same MOF could give us qualitative information, as discussed later.

## 3. Results

**3.1. Experimental Issues: MOF Perturbation by Guest Molecules and Hydrogen Detection.** To characterize the interaction of hydrogen within different MOFs, it is first necessary to measure the effect of host molecules within the MOF on the MOF structure which will affect the MOF's combination bands appearing in the $H_2$ stretch spectral range (4000−4500 $cm^{-1}$). The changes in the MOF IR absorption spectra have therefore been examined in high-pressure environments using different gases, such as helium (monatomic gas) and deuterium (chemically identical to hydrogen). Both helium and deuterium have an atomic mass different from that of hydrogen, and the fundamental stretch frequency of ortho $D_2$ is at 2983 $cm^{-1}$, far away from the hydrogen region of interest (>4000 $cm^{-1}$). Therefore, deuterium can be used as a reference to get a clean signal for hydrogen, without interference from MOF-induced IR absorption.

The use of deuterium is particularly important because the hydrogen stretch vibrational and vibrational−rotational modes

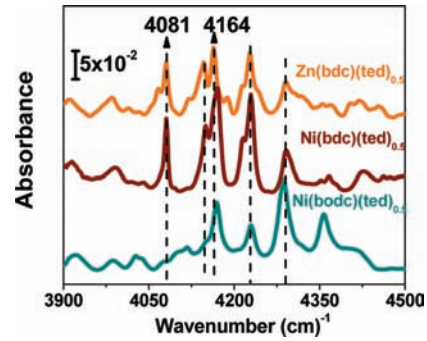


***Figure 1.*** IR absorption spectra (KBr reference subtracted) of activated $M(bdc)(ted)_{0.5}$ (M = Ni, Zn) and $Ni(bodc)(ted)_{0.5}$ in a vacuum. Exchanging Ni for Zn causes a blue shift of the $\nu$(C−C) mode at 4164 $cm^{-1}$, where the C−C entity is connected to the $Zn_2(COO)_4(ted)_2$ paddle-wheel SBU. The IR band at 4081 $cm^{-1}$ is solely due to the bdc ligand and therefore is absent in the $Ni(bodc)(ted)_{0.5}$ absorption spectrum.

are in a spectral region (4000−5000 $cm^{-1}$) where MOFs have detectable absorption features. Indeed, both overtones and combination bands of the MOF ligand modes are located in the near-IR (NIR) region as a result of mechanical and electrical anharmonicities of the system. Typically NIR bands have much weaker intensities relative to fundamentals in the mid-IR bands. Such anharmonicities are typically on the order of 1−3%, and the MOF spectrum in the 4000−4500 $cm^{-1}$ is dominated by bands arising from X−H bonds.[59]

The measured spectra of the MOFs are composed of combination bands of $\nu$(C−C) and $\nu$(C−H) of the MOFs' backbone as shown in Figure 1 for $M(bdc)(ted)_{0.5}$ and $Ni(bodc)(ted)_{0.5}$. While assignment of these spectral features is difficult, comparison between closely related systems can help identify the chemical group responsible for the absorption. For instance, comparing the combination bands of both bdc and bodc systems, the absence of the vibration frequency at 4081 $cm^{-1}$ for $Ni(bodc)(ted)_{0.5}$ indicates that this IR band is related to the $\nu$(C−C) and $\nu$(C−H) combination bands of the benzene ring in the benzenedicarboxylate ligand. In addition, the absence of vibrational absorption at 4358 $cm^{-1}$ in the $M(bdc)(ted)_{0.5}$ system indicates that this IR band is related to $\nu$(C−C) and $\nu$(C−H) combination bands of the bodc ligand present in $Ni(bodc)(ted)_{0.5}$. Interestingly, there exists a 5 $cm^{-1}$ blue shift of the IR vibrational band at 4164 $cm^{-1}$ for $Zn(bdc)(ted)_{0.5}$ when the metal center is replaced by nickel. This indicates that this IR combination band is that of $\nu$(C−C) that is connected to the $Zn_2(COO)_4(ted)_2$ paddle-wheel SBU. The shift to higher wavenumbers is attributed to the increase of electronegativity of the metal center when zinc (1.65) is substituted with nickel (1.91). Similar shifts are observed for the M−formate systems, when the manganese or cobalt metal centers are replaced with nickel. The $\nu$(C−H) IR band in the COOH connected to the metal center at 4255 $cm^{-1}$ undergoes an 8 $cm^{-1}$ blue shift as shown in Figure S5 in the Supporting Information. In general, the presence of the MOFs' combination bands with an intensity of $\sim 10^{-2}$ in this region introduces a difficulty in IR analysis of the hydrogen absorption spectra, particularly when these bonds are perturbed by the presence of the guest molecule.

To quantify the effect that guest molecules have on the MOF structure, IR measurements were performed using different probing gases such as helium, deuterium, and hydrogen over

(54) Gonze, X.; et al. *Comput. Mater. Sci.* **2002**, *25*, 478–492.
(55) Gonze, X.; et al. *Z. Kristallogr.* **2005**, *220*, 558–562.
(56) Ordejón, P.; Artacho, E.; Soler, J. M. *Phys. Rev. B* **1996**, *53*, R10441.
(57) Soler, J. M.; Artacho, E.; Gale, J. D.; Garcia, A.; Junquera, J.; Ordejon, P.; Sanchez-Portal, D. *J. Phys.: Condens. Matter* **2002**, *14*, 2745–2779.
(58) Troullier, N.; Martins, J. L. *Phys. Rev. B* **1991**, *43*, 1993.
(59) Siesler, H. W.; Ozaki, Y.; Kawata, S.; Heise, H. M. *Near Infrared Spectroscopy*; Wiley-VCH: New York, 2002.

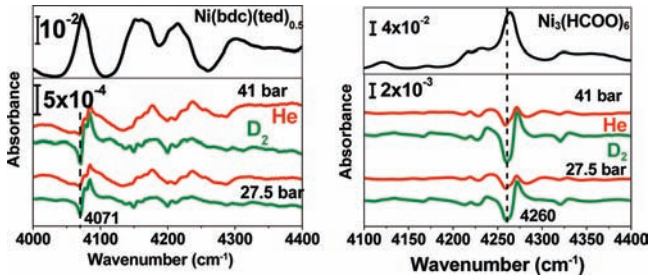


***Figure 2.*** IR absorption spectra of (top, left) activated Ni(bdc)(ted)$_{0.5}$ in a vacuum absorption referenced to KBr in a vacuum and (bottom, left) Ni(bdc)(ted)$_{0.5}$ by helium (red) and deuterium (green) gases referenced to activated Ni(bdc)(ted)$_{0.5}$ in a vacuum. The top right part shows the IR absorption spectra of activated $Ni_3(HCOO)_6$ in a vacuum referenced to KBr in a vacuum, and the bottom right part shows the perturbed structure of $Ni_3(HCOO)_6$ due to helium (red) and deuterium (green) gases. Larger shifts of $\sim$+12 cm$^{-1}$ are observed for $Ni_3(COOH)_6$.

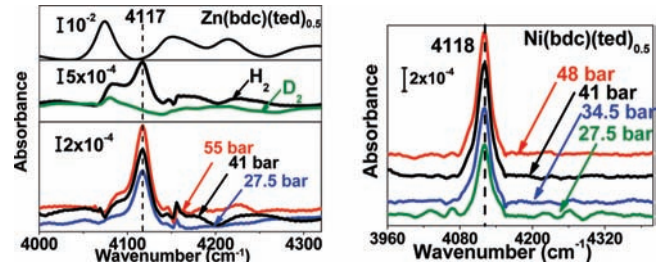


***Figure 3.*** IR absorption spectra (top, left) of activated Zn(bdc)(ted)$_{0.5}$ in a vacuum referenced to KBr in a vacuum. The middle left part shows Zn(bdc)(ted)$_{0.5}$ exposed to hydrogen and deuterium at 55 bar both referenced to Zn(bdc)(ted)$_{0.5}$ in a vacuum and the bottom left part difference spectra of hydrogen and deuterium. The right part shows difference absorption spectra of hydrogen and deuterium for activated Ni(bdc)(ted)$_{0.5}$ both referenced to Ni(bdc)(ted)$_{0.5}$ in a vacuum.

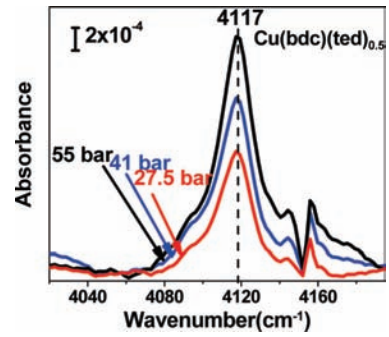


***Figure 4.*** Difference spectra of hydrogen and deuterium for Cu(bdc)(ted)$_{0.5}$ for different pressures showing the appearance of a hydrogen IR band at 4117 cm$^{-1}$ and an fwhm of $\sim$20 cm$^{-1}$.

the range of 27−55 bar. Figure 2 shows that the MOF combination bands of Ni(bdc)(ted)$_{0.5}$ and $Ni_3(HCOO)_6$ are affected by the guest molecules, exhibiting a blue shift upon guest incorporation. The magnitude of the blue shift and of the modulated intensities depends on the particular MOF structure. For instance, the top part of Figure 2 shows the combination bands of activated Ni(bdc)(ted)$_{0.5}$ (left) and $Ni_3(HCOO)_6$ (right) in a vacuum ($10^{-4}$ Torr). The bottom part of Figure 2 shows absorption spectra after loading helium (red) and deuterium (green), referenced to activated Ni(bdc)(ted)$_{0.5}$ and $Ni_3(HCOO)_6$ in a vacuum, respectively. Derivative-like features in the absorption spectra appear due to a 6 cm$^{-1}$ blue shift of the Ni(bdc)(ted)$_{0.5}$ combination band at 4081 cm$^{-1}$ assigned to $\nu$(C−C) and $\nu$(C−H) in the benzene ring when exposed to helium and deuterium gases. For comparison, Ni(bodc)(ted)$_{0.5}$ shows a 14 cm$^{-1}$ shift of the IR band corresponding to the bodc ligand at 4358 cm$^{-1}$ with intensities similar to those of the Ni(bdc)(ted)$_{0.5}$ system (data not shown). Blue shifts of $\sim$12 cm$^{-1}$ with larger intensities are observed for $\nu$(C−H) connected to the C−O bond attached to the metal centers in 1-D small pore formate MOFs when exposed to both deuterium and helium gases as shown in Figure 2 (right). The degree of perturbation of the MOFs can be quantified by normalizing the derivative intensities for the different MOFs to the initial absorbance of the MOF combination band spectrum. This exercise reveals that the perturbation increases (i.e., the normalized differential intensity is higher) when the pore size decreases. Indeed, higher intensities are observed for small 1-D pore structure MOFs with one type of ligand (i.e., formate) compared with larger pore MOFs. Finally, if hydrogen is incorporated instead of deuterium or helium, similar derivative-like features are observed and a new absorption feature appears which is not related to the MOF combination band spectrum. This feature can therefore be unambiguously associated with the perturbed H−H stretch of hydrogen incorporated into the MOF micropores.

The procedure to extract a clean IR absorption spectrum for hydrogen in MOFs is therefore to use the spectrum of deuterium incorporated at the same pressure as the reference, as shown in Figure 3 for instance for Zn(bdc)(ted)$_{0.5}$ and Ni(bdc)(ted)$_{0.5}$. These spectra are shown and discussed in the next section.

**3.2. Infrared Absorption Spectra of Hydrogen in Four Types of MOFs. 3.2.1. M(bdc)(ted)$_{0.5}$.** Samples with M = Zn, Ni, and Cu show $\Delta\nu$(H−H,ortho) $\approx$ −38 cm$^{-1}$ for Zn(bdc)(ted)$_{0.5}$ and Cu(bdc)(ted)$_{0.5}$ and $\Delta\nu$(H−H,ortho) $\approx$ −37 cm$^{-1}$ for Ni(bdc)(ted)$_{0.5}$ with an fwhm of $\sim$20 cm$^{-1}$ for Zn(bdc)(ted)$_{0.5}$, Cu(bdc)(ted)$_{0.5}$ and Ni(bdc)(ted)$_{0.5}$ as shown in Figures 3 and 4. The top left part of Figure 3 shows the spectrum of Zn(bdc)(ted)$_{0.5}$ activated in vacuum ($10^{-4}$ Torr), and the middle part shows both hydrogen and deuterium absorption spectra upon exposures to 55 bar of hydrogen and deuterium gases; the spectra are referenced to Zn(bdc)(ted)$_{0.5}$ activated in a vacuum. The bottom part shows the difference between hydrogen and deuterium absorptions at identical pressures. Figures 3 (right) and 4 show the difference spectra of hydrogen and deuterium for Ni(bdc)(ted)$_{0.5}$ and Cu(bdc)(ted)$_{0.5}$. The small interference feature at 4155 cm$^{-1}$ (most evident in Figure 4) is associated with hydrogen incorporated in mesoporous ($\sim$20 nm) regions as discussed in section 4.2.

**3.2.2. Ni(bodc)(ted)$_{0.5}$.** Changing the aromatic ligand (bdc) in Ni(bdc)(ted)$_{0.5}$ to an aliphatic ligand (bodc) while keeping the same metal center generates an identical structure with a slightly smaller pore size of $\sim$7 Å. Despite the similarity in structures of the bdc and bodc MOFs, the shift of the ortho $\nu$(H−H) IR band is measurably smaller ($\sim$−34 cm$^{-1}$) than for the bdc MOF, with an fwhm of 32 cm$^{-1}$ as shown in Figure 5. As discussed below, the line widths in the IR absorption of $H_2$ are mostly due to inhomogeneities. The measured shifts, however, indicate that $H_2$ interacts more weakly with the bodc ligand than the bdc ligand.

**3.2.3. $M_3(HCOO)_6$.** Infrared measurements performed on 1-D pore structures such as $M_3(HCOO)_6$ (M = Ni, Mn, Co) show shifts of the $H_2$ stretch band that are significantly smaller (−28 and −30 cm$^{-1}$) than for the 3-D pore MOFs studied above. The hydrogen IR bands are now at 4125 cm$^{-1}$ for $Ni_3(HCOO)_6$ and at 4127 cm$^{-1}$ for $Mn_3(HCOO)_6$ and $Co_3(HCOO)_6$ as shown in Figures 6 and 7. In addition, all metal−formate (M−Fa) systems show a significantly narrower fwhm of 13 cm$^{-1}$ as

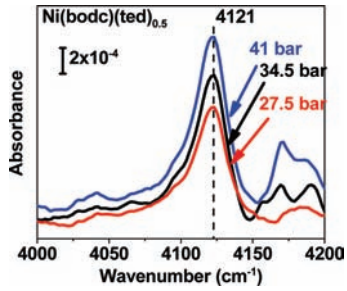


***Figure 5.*** Difference spectra of hydrogen and deuterium for activated $Ni(bodc)(ted)_{0.5}$ showing a $-34$ $cm^{-1}$ red shift of the ortho H vibration with an fwhm of 32 $cm^{-1}$.

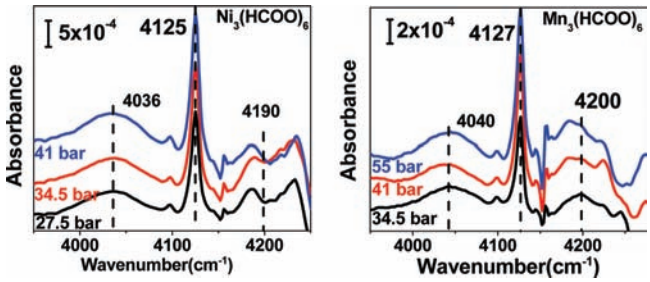


***Figure 6.*** Difference absorption spectra of hydrogen and deuterium for $Ni_3(HCOO)_6$ (left) and $Mn_3(HCOO)_6$ (right), with $\Delta\nu$(H−H,ortho) = 30 and 28 $cm^{-1}$, respectively, and an fwhm of 13 $cm^{-1}$, and the ppearance of frustrated translational states $\sim\pm100$ $cm^{-1}$ from the shifted $H_2$ fundamental ortho $H_2$ vibration. The MOF perturbation in this region causes the loss bands to be less enhanced.

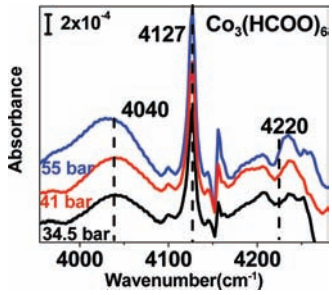


***Figure 7.*** Difference spectra of hydrogen and deuterium for $Co_3(HCOO)_6$ at different pressures showing a $H_2$ IR band similar to that of $Mn_3(HCOO)_6$ at 4127 $cm^{-1}$ with an fwhm of 13 $cm^{-1}$ and the appearance of translational states $\sim\pm100$ $cm^{-1}$ away from the shifted $H_2$ IR band. Again the loss band is less enhanced due to the MOF perturbation in this region.

summarized in Table 1. Other spectral features can be associated with $H_2$. Despite interference from miscancellations of MOF combination bands in the 4150−4250 $cm^{-1}$ region, two broad bands are apparent on either side (i.e., centered at $\sim\pm100$ $cm^{-1}$ around the fundamental ortho $H_2$ stretch band). These two bands are centered at 4036 $cm^{-1}$ for $Ni_3(HCOO)_6$ and 4040 $cm^{-1}$ for $Mn_3(HCOO)_6$ and $Co_3(HCOO)_6$ on the gain side and at $\sim$4200 $cm^{-1}$ for all three materials on the loss side. The loss bands are not as well-defined because they are obscured by the perturbations of the MOF combination bands. These broad bands are attributed to the frustrated translational states of $H_2$ molecules trapped in small pores by even smaller apertures at the apex connecting the 1-D zigzag-shaped channels. Previous observations of translational states have been reported for $H_2$ in MOF-5 and fullerenes at low temperatures using diffuse reflectance infrared spectroscopy.[60,61]

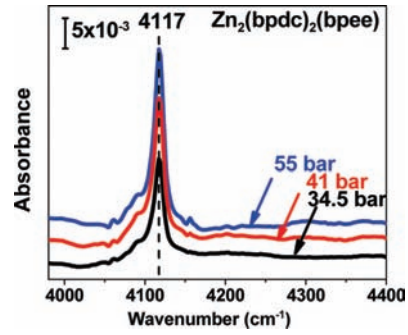


***Figure 8.*** Difference absorption spectra of hydrogen and deuterium for $Zn_2(bpdc)_2(bpee)$ at different pressures showing a hydrogen IR band at 4117 $cm^{-1}$ and an fwhm of 16 $cm^{-1}$ with an intensity much larger than that of the other systems.

**3.2.4. $Zn_2(bpdc)_2(bpee)$.** For $Zn_2(bpdc)_2(bpee)$, a 1-D pore complex structure with interpenetrating lattices and relatively smaller pores, the $H_2$ stretch spectrum is characterized by an intense ortho $\nu$(H−H) IR band at 4117 $cm^{-1}$, i.e., with a shift of $\sim-38$ $cm^{-1}$ (Figure 8). The shift of the H−H stretch mode is typical of $H_2$ interacting with benzene rings (i.e., similar to shifts observed in $M(bdc)(ted)_{0.5}$). However, the IR absorption intensity is significantly larger ($\sim10\times$) and the fwhm smaller (16 $cm^{-1}$) than for $H_2$ in $M(bdc)(ted)_{0.5}$.

These observations suggest that the magnitudes of the $H_2$ stretch frequency shifts, intensities, and even line- widths contain important information about the nature of the $H_2$ interaction in the pores and depend on the structure and chemical nature of the MOF hosts. These parameters are summarized in Table 1 and examined in the next section.

The integrated intensities of the $\nu$(H−H) IR absorption bands for all the MOFs studied above increase linearly with increasing pressure as shown in Figure 9. The linear behavior confirms that this band is not due to $H_2$ *gas* (which would increase quadratically with pressure),[42] but to $H_2$ trapped in the pores. Indeed, this pressure dependence is similar to the linear dependence observed in the isotherm measurements at room temperature as shown in Figure S4 (Supporting Information). The left panel of Figure 9 clearly shows that the integrated areas of the $M(bdc)(ted)_{0.5}$ and $Ni(bodc)(ted)_{0.5}$ systems are comparable and slightly larger than those of the M−Fa systems. The largest area is that of the $Zn_2(bpdc)_2(bpee)$ system. Since

***Table 1.*** Comparison between the Different Properties of the Different Studied MOFs

| MOF | ligand type | $\Delta\nu$(H−H) ($cm^{-1}$) | fwhm ($cm^{-1}$) | structural perturbation ($cm^{-1}$) | pore structure/size (Å) | binding energy (kJ/mol) |
|---|---|---|---|---|---|---|
| $Zn(bdc)(ted)_{0.5}$ | aromatic, aliphatic | −38 | 20 | 5 | 3-D/$\sim$7.8[43] | 5−5.3[43] |
| $Ni(bdc)(ted)_{0.5}$ | aromatic, aliphatic | −37 | 20 | 6 | NA | NA |
| $Cu(bdc)(ted)_{0.5}$ | aromatic, aliphatic | −38 | 20 | 8 | 3-D/$\sim$7.8[43] | 4.9−6.1[43] |
| $Ni(bodc)(ted)_{0.5}$ | aliphatic | −34 | 32 | 14 | 1-D/$\sim$7−7.3[44] | 5.7−6.5[30] |
| $Ni_3(COOH)_6$ | short aliphatic | −30 | 13 | 12 | 1-D/$\sim$5−6[45] | 8.3−6.5[45] |
| $Mn_3(COOH)_6$ | short aliphatic | −28 | 13 | 14 | 1-D/$\sim$5−6[45] | NA |
| $Co_3(COOH)_6$ | short aliphatic | −28 | 12 | 13 | NA | NA |
| $Zn_2(bpdc)_2(bpee)$ | aromatic | −38 | 16 | 10 | 1-D/$\sim5\times7$[6] | 9.5 (viral),[6] 8.8 (poly)[6] |

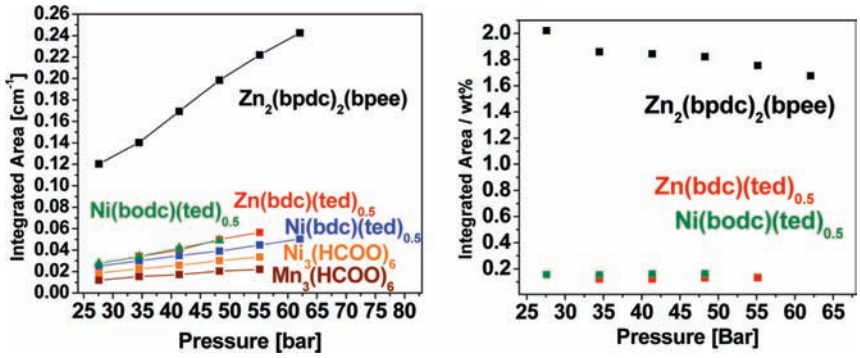


***Figure 9.*** Integrated areas of hydrogen IR bands for the different MOFs as a function of pressure (left) and normalized integrated areas by the concentration (wt %) of hydrogen adsorbed from isotherm measurements (right). Much higher, ~10 times, intensities are observed for $Zn_2(bpdc)_2(bpee)$.

***Table 2.*** Comparison between the Normalized Integrated Areas for the Three MOF Systems

| MOF | hydrogen concn (wt %) at 41 bar (RT isotherm) | integrated area (cm$^{-1}$) at 41 bar | normalized integrated area intensity/wt % |
|---|---|---|---|
| $Zn(bdc)(ted)_{0.5}$ | 0.327 | 0.0401 | 0.1224 |
| $Ni(bodc)(ted)_{0.5}$ | 0.26 | 0.0419 | 0.1604 |
| $Zn_2(bpdc)_2(bpee)$ | 0.0918 | 0.1693 | 1.8436 |

the areas are proportional to the amount of $H_2$ incorporated in the MOFs, it is important to normalize the measured IR integrated areas by the concentration (wt %) of hydrogen uptake at room temperature derived from isotherm measurements. Isotherm measurements were therefore performed for $Zn(bdc)(ted)_{0.5}$, $Ni(bodc)(ted)_{0.5}$, and $Zn_2(bpdc)_2(bpee)$, and the data taken at 41 bar are shown in Table 2. The normalized integrated intensities shown in the right panel of Figure 9 and summarized in Table 2 show that both $Zn(bdc)(ted)_{0.5}$ and $Ni(bodc)(ted)_{0.5}$ have similar absorption per $H_2$ molecule. In contrast, the IR absorption of $H_2$ in $Zn_2(bpdc)_2(bpee)$ is approximately 10 times that of the other compounds.

The results summarized in Tables 1 and 2, including IR vibrational shifts, fwhm, and guest-induced shifts, differences in structure, pore sizes, and binding energies, and normalized intensities, show that there is no correlation between the binding energies for each MOF and the hydrogen vibrational band IR shifts. Results for the M−Fa systems that have the highest binding energies (lowest surface area, 304 m$^2$/g) among the MOFs studied here show the lowest hydrogen IR shifts. Similarly, a recent study performed at 77 K has shown that hydrogen uptake for pressures >~0.5 bar is influenced by the specific surface area and not by the binding energies, as is the case for the lower pressure regions.[62]

## 4. Discussion

**4.1. Interaction of Guest Molecules with the MOF Ligands.** Figure 2 gives clear spectroscopic evidence that the introduction of a guest molecule (He, $D_2$, $H_2$) into the MOF system through high-pressure loading induces a blue shift in the absorption features of the MOF combination bands. This shift is a result of the distortion in the bonds of the MOF backbone (ligands). Two observations help identify the interaction between the guest molecules and the MOF. First, the IR band that is most affected at 4081 cm$^{-1}$ is related to the C−C and C−H combination bands of the benzene ring in the $M(bdc)(ted)_{0.5}$ backbone, suggesting that the benzene ring might be the most affected by guest molecules and/or that the perturbation of the benzene ring leads to the strongest spectral changes. Second, the strength of the interaction depends on the guest molecules. Specifically, the perturbation of the band at 4081 cm$^{-1}$ is twice as strong with deuterium as with He. Since He is heavier than $D_2$, the perturbation of the benzene ring must be dominated by the dispersion forces between the guest molecule and C−H bonds. Indeed, the electric polarizability of deuterium ($\alpha = 0.61$ fm$^3$) is much higher than that of helium ($\alpha = 0.072$ fm$^3$).[63] Furthermore, hydrogen and deuterium both have the additional contribution of a permanent quadrupole moment, which is absent in the case of helium. Therefore, the perturbation of the ligand is dominated by dispersion forces between the guest and ligand, rather than by mechanical forces (hard wall potential).

All the MOFs studied have structural perturbations induced by guest molecules, which are stronger for molecules ($H_2$, $D_2$) that are more polar than He. In the case of the $M(bdc)(ted)_{0.5}$ structures, the most perturbed bands correspond to C−C and C−H of the benzene ring in the bdc ligand. However, the perturbation in the $M(bdc)(ted)_{0.5}$ systems is less significant than for the other MOFs studied, as shown in Table 1, indicating that the benzene ring is less polarizable than the ligands in the other MOFs, leading to smaller shifts. In addition, the highest perturbation intensity is for the M−Fa system, due to the type of ligand and pore size in this structure.

Since the interaction is dominated by dispersion forces, it becomes apparent that the effects on the MOF combination modes can be minimized when measuring the vibrational spectra of $H_2$ by using the same pressure of $D_2$ (instead of He) in the MOF as the reference.

**4.2. Interaction of Hydrogen with the MOFs.** The nature of the interaction between $H_2$ and the MOF can be further investigated by examining the $H_2$ stretch spectrum. Hydrogen molecules are IR inactive and exist as two isomers with different nuclear spins. Para $H_2$ is characterized by a nuclear singlet state and ortho $H_2$ by a nuclear triplet state. The two states have different rotational transitions as dictated by selection rules, which give rise to distinguishable IR frequencies. The transitions from $\nu = 0$ to $\nu = 1$ for para Q(0) and ortho Q(1) states are at 4161 and 4155 cm$^{-1}$, respectively. At room temperature the equilibrium composition for ortho:para is 3:1 and consists of S lines that are due to quadrupolar induction. The Q branch is characterized by two maxima, $Q_p$ and $Q_R$, arising from an intercollisional interference effect as shown in Figure S3 (Supporting Information).[42] The intensity of pure hydrogen gas increases quadratically with pressure.[42]

In contrast, the intensity of the IR hydrogen band due to the interaction with the MOFs' adsorption sites increases linearly with pressure. This indicates that there is a negligible $H_2$−$H_2$ interaction in the MOF system. Moreover, the magnitude of

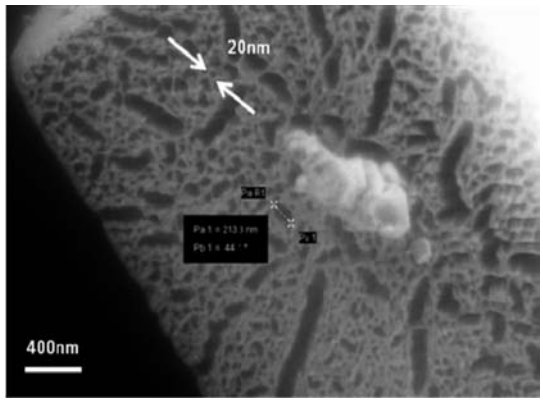


***Figure 10.*** SEM image of Ni(bdc)(ted)$_{0.5}$ showing macro- and mesopores ranging from ~20 to 200 nm. The small pores of 20 nm are believed to cause the shift on the Q dip in gaseous $H_2$. This is caused by the perturbation of the gas phase by the MOF walls affecting the IR activity of the gas phase induced by intercollision interference.

the $H_2$ stretch band fwhm depends on the interaction energy dispersion from the different adsorption sites, if inhomogeneities are negligible. The IR absorption intensity, on the other hand, depends on the magnitude and symmetry of the interaction within the specific site in the structure.

Much can be learned from first-principles calculations as detailed below. Before discussion of these calculations, a derivative-looking feature at 4155 cm$^{-1}$, most apparent in Figure 4, is considered. This feature occurs at the position of the collision-induced interference "dip" of gas-phase $H_2$ as shown in Figure S3 (Supporting Information)[42] and is not completely eliminated by subtracting the $H_2$ spectrum taken at the same pressure. This behavior suggests that there is $H_2$ gas trapped in micro- and mesopores in the vicinity of the MOF (i.e., not inside the MOF itself). If the size of such defects is smaller than ~<50 nm, then the spectrum of the $H_2$ gas will be measurably perturbed by its interaction with the defect internal surfaces, as is the case for $H_2$ in H:a-Si for instance.[64] This interaction is pressure dependent because the MOF's structure deforms slightly under pressure. Interestingly, such micro- and mesosize defects have been identified in SEM pictures and appear to be present in otherwise crystalline MOFs as shown in Figure 10. Such pores are in large enough quantities when MOF crystallites are lightly pressed on KBr pellets to produce a measurable change in the sharpest part of the gas-phase spectrum, namely, the intercollisional dip at 4155 cm$^{-1}$.

To understand the MOF−$H_2$ interaction and the effect of metal substitution, we performed vdw-DF calculations for M(bdc)(ted)$_{0.5}$ (M = Zn and Cu). Figure 11 shows the adsorption sites in the system. Two types of binding sites are located. One is at the face center of the bdc−ted plane with bond orientation perpendicular to the plane. The other is near the corner and aligned somewhat along the body diagonal of the cell, as shown in Figure 11 (right). These results are consistent with our previously published data.[65] Furthermore, we located all four corner sites that are not completely symmetrical to each other, due to the 3-fold rotational symmetry of the ted molecule. It can be seen that the two hydrogen atoms at the face center site are more symmetrical to each other than at corner sites. Therefore, the induced dipole moment and correspondingly the IR cross section is expected to be much larger for $H_2$ in the corner-adsorbing site. An estimation based on the integration of the dipole difference due to $H_2$ over the unit cell shows that the IR cross section for the face center case is about 2 orders of magnitude smaller, although the interaction between neighboring cells makes this estimation a very crude approximation. As such, the IR spectrum mainly arises from the corner site adsorbed $H_2$. Table 3 shows the calculated frequency shifts of the four corner sites and the binding energy at each position in Zn(bdc)(ted)$_{0.5}$. A shift of −32 cm$^{-1}$ is observed for the strongest binding position, 1b, and is reasonably consistent with the measured value of −38 cm$^{-1}$, while a standard generalized gradient approximation (GGA) calculation gives a shift of −21 cm$^{-1}$ with a much smaller binding energy of −2.5 kJ/mol at site 1a.

M(bdc)(ted)$_{0.5}$ MOFs made of 3-D pore structures show no dependence of the hydrogen IR vibrational shifts on metal substitution, as confirmed by vdW-DF calculations. As shown in Table 3, the frequency shift at site 1a in Cu(bdc)(ted)$_{0.5}$ is 26 cm$^{-1}$ compared to 29 cm$^{-1}$ in Zn(bdc)(ted)$_{0.5}$. This is different from the MOF with unsaturated metal atoms where the frequency shift is very sensitive to the metal species. In M(bdc)(ted)$_{0.5}$, the metal atoms form 6-coordinated bonds and are fully shielded. The H−M distance is about 4 Å for the corner sites (much further away for the face center sites), while the H−oxygen distance is about 3 Å. There is probably some overestimation (~0.3 Å) in these calculated distances, which is typical in vdW-DF calculations. To bring the hydrogen molecule closer to the metal atom would lead to an even shorter H−O distance where repulsion becomes important and the state is energetically unfavorable. The calculations also show that the H−H bond preferentially points toward the metal atom, as shown in Figure 12. This is in contrast with the adsorption to the unsaturated metal sites in MOF-74 where the H−H bond tends to align perpendicular to the metal−H axis such that both H atoms get maximum interaction with the metal. In fact, Figure 12 shows that the perpendicular orientation of the H−H bond to the metal−H axis in M(bdc)(ted)$_{0.5}$ is the weakest, which suggests that hydrogen interaction with the metal atom is less important than with the bdc linker. As such, calculations show negligible effects upon substituting the Zn atom with Cu, in agreement with experiments.

In addition, smaller IR vibrational shifts are observed when exchanging the aromatic with an aliphatic ligand as shown in Table 1 for Ni(bdc)(ted)$_{0.5}$ and Ni(bodc)(ted)$_{0.5}$. The fwhm's in these systems are ~20 cm$^{-1}$ for Ni(bdc)(ted)$_{0.5}$ and ~32 cm$^{-1}$ for Ni(bodc)(ted)$_{0.5}$. This width is attributed to the combination of different adsorption sites and other inhomegenieties of the system. Only sites with the highest interactions (largest binding energies) and largest asymmetry contribute most to the IR absorption spectrum. Therefore, the hydrogen IR absorption band measured at room temperature in M(bdc)(ted)$_{0.5}$ is dominated by the interaction with the benzene ring ligand, rather than by $H_2$ in the minority of the sites (next to the triethylenediamine ligand). In addition, for the M(bdc)(ted)$_{0.5}$ system, the most perturbed IR band is at 4081 cm$^{-1}$ corresponding to the C−C and C−H of the benzene ring. Although the binding energies depend on the proximity of the organic ligands, giving

(60) Herman, R. M.; Lewis, J. C. *Physica B* **2009**, *404*, 1581–1584.
(61) FitzGerald, S. A.; Allen, K.; Landerman, P.; Hopkins, J.; Matters, J.; Myers, R.; Rowsell, J. L. C. *Phys. Rev. B: Condens. Matter* **2008**, *77*, 224301.
(62) Hirscher, M.; Panella, B.; Schmitz, B. *Microporous Mesoporous Mater.* [Online early access]. DOI: 10.1016/j.micromeso.2009.06.005. Published Online: June 11, 2009.
(63) Stetcu, I.; Quaglioni, S.; Friar, J. L.; Hayes, A. C.; Petr, N. *Phys. Rev. C: Nucl. Phys.* **2009**, *79*, 064001.
(64) Chabal, Y. J.; Patel, C. K. N. *Phys. Rev. Lett.* **1984**, *53*, 1771–1774.

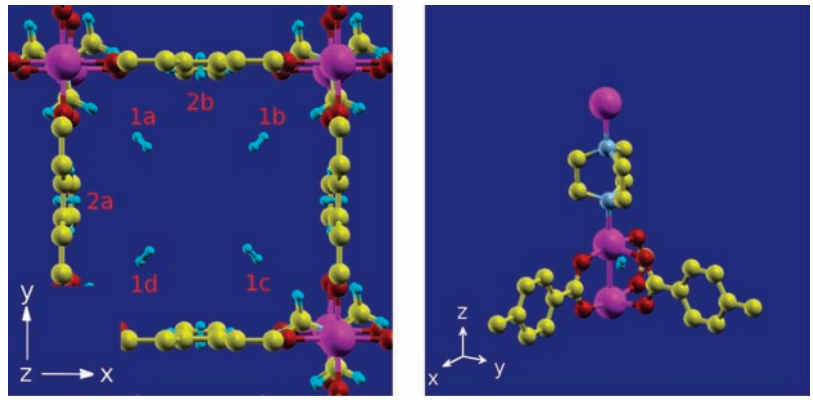


***Figure 11.*** (Left) Adsorption sites in M(bdc)(ted)$_{0.5}$ and (right) adsorption site 1a.

***Table 3.*** Calculated Frequency Shifts for the Four Corner Sites and Binding Energies at Each Position for Zn(bdc)(ted)$_{0.5}$ and Cu(bdc)(ted)$_{0.5}$

| MOF | site | $\Delta\nu$(H−H) (cm$^{-1}$) | binding energy[a] (kJ/mol) |
|---|---|---|---|
| Zn(bdc)(ted)$_{0.5}$ | 1a | −29 | −10 |
| | 1b | −32 | −10.4 |
| | 1c | −25 | −9.9 |
| | 1d | −26 | −10 |
| Cu(bdc)(ted)$_{0.5}$ | 1a | −26 | −9.8 |

[a] These binding energies do not include the zero-point energy (ZPE) or thermal corrections, which are typically about 3 kJ/mol in MOF systems.[65,66] Better agreement with the experimental Qst will be obtained after such corrections are made.

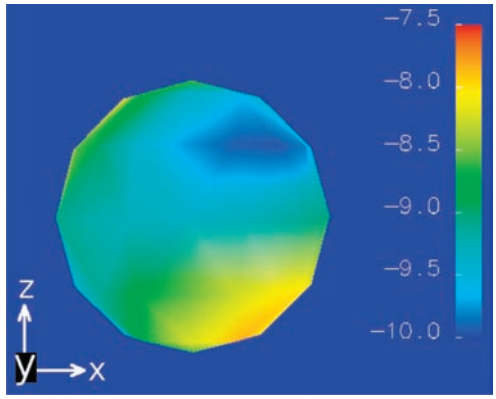


***Figure 12.*** Orientational dependence of the potential (kJ/mol) at adsorption site 1a. The minimum position corresponds to the equilibrium orientation shown in Figure 11 (right).

Ni(bodc)(ted)$_{0.5}$ a higher binding energy than Ni(bdc)(ted)$_{0.5}$, our data show that the hydrogen IR bands are more shifted for Ni(bdc)(ted)$_{0.5}$ than Ni(bodc)(ted)$_{0.5}$. These results suggest that the shifts observed in the H−H stretch modes are sensitive to the nature of individual ligands, and are not correlated to the magnitude of the binding energies. Ligands with $\pi$-electrons lead to the largest shifts.

For small 1-D pore structure systems such as M−Fa, exchanging metal centers can affect the magnitude of the H−H stretch frequency. For instance, there is a 2 cm$^{-1}$ blue shift when nickel is exchanged with manganese or cobalt, as shown in Figures 6 and 7. The electronegativity of nickel is higher (1.91) than that of manganese (1.55) but similar to that of cobalt (1.88). However, Figure S5 in the Supporting Information shows that the IR combination band at 4163 cm$^{-1}$ is most shifted (∼8 cm$^{-1}$) for Ni−Fa (not for Co−Fa even with a relatively small electronegativity difference). In contrast to the other MOFs studied here, the M−Fa system has the metal atom in close proximity of the ligands. Therefore, the nature of the metal can affect the ligands and slightly modify the overall MOF geometry (pore size). Since the Ni−Fa system has the smallest unit cell among the M−Fa systems (the nickel ion radius is the smallest (0.83 Å)), the electronegativity of nickel is sufficient to affect the ligands and therefore create an environment for $H_2$ different from that of the cobalt and manganese MOFs. Thus, the hydrogen interaction is stronger for nickel than for manganese or cobalt, which causes a larger $H_2$ stretch shift.

Table 1 also shows that the fwhm in these systems is narrower than that in the M(bdc)(ted)$_{0.5}$ systems. This may be due to the nature of the system (with only one type of organic ligand, formate), which tends to limit the range of inhomogeneities. Although the binding energies for the Mn− and Co−formate MOFs are not available, the present results are consistent with the fact that it is the nature of the chemical environment (changed by metal substitution) that affects the H−H vibrational frequency, rather than the energy required to remove $H_2$ from the pores.

Interestingly, translational states are observable ∼±100 cm$^{-1}$ away from the $H_2$ stretch band. This result suggests that the anharmonic coupling between the frustrated translational and H−H stretch modes is stronger for smaller 1-D pore structured MOFs with 1-D interconnected channels. The appearance of these bands results from entrapment of the molecules within the pore, due to small apertures connecting these 1-D channels. The magnitude of the frustrated translation modes is consistent with what was calculated for Zn(bdc)(ted)$_{0.5}$ where the calculated translational frequencies along the $x$, $y$, and $z$ directions at the corner site 1a are 110, 120, and 90 cm$^{-1}$ respectively, as shown in Figure 13, although for this system the sidebands are not detectable. Similar translational frequencies have also been observed for $H_2$ in $C_{60}$ (110 cm$^{-1}$) and in HKUST-1 (90 cm$^{-1}$).[67,68] The fact that these modes can be most easily detected in the M−Fa system suggests that the size of the aperture

(65) Kong, L.; Cooper, V. R.; Nijem, N.; Li, K.; Li, J.; Chabal, Y. J.; Langreth, D. C. *Phys. Rev. B: Condens. Matter* **2009**, *79*, 081407.
(66) Kong, L.; Roman-Perez, G.; Soler, J. M.; Langreth, D. C. *Phys. Rev. Lett.* **2009**, *103*, 096103.
(67) FitzGerald, S. A.; Churchill, H. O. H.; Korngut, P. M.; Simmons, C. B.; Strangas, Y. E. *Phys. Rev. B: Condens. Matter* **2006**, *73*, 155409.
(68) Bordiga, S.; Regli, L.; Bonino, F.; Groppo, E.; Lamberti, C.; Xiao, B.; Wheatley, P. S.; Morris, R. E.; Zecchina, A. *Phys. Chem. Chem. Phys.* **2007**, *9*, 2676–2685.

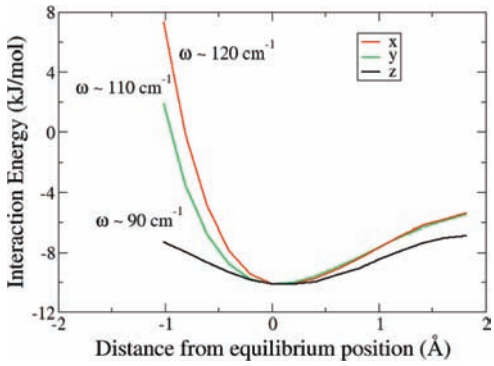


***Figure 13.*** Potential and frequencies of the translational movement of $H_2$ at site 1a along the *x*, *y*, and *z* directions.

connecting pores can affect the anharmonic coupling between translational and vibrational modes.

The $Zn_2(bpdc)_2(bpee)$ 3-D framework also contains a 1-D pore structure similar to that of the M−Fa system but with aromatic carboxylate ligands rather than formates. Consequently, the $H_2$ stretch shifts are similar to those observed in the $M(bdc)(ted)_{0.5}$ systems. For this system, calculations estimate shifts (45 $cm^{-1}$) that are larger than experimentally measured. The discrepancy has been discussed by Lan et al.[6] and is attributed to the fact that the structure used in the calculations (based on X-ray measurements of the MOF prior to activation) is probably not the same as the structure obtained after activation (used for $H_2$ loading experiments). Unfortunately, while X-ray diffraction shows a difference, the full structure determination of the activated MOF has not yet been successfully performed.

Figure 9 shows that the integrated areas measured for $M(bdc)(ted)_{0.5}$ and $Ni(bodc)(ted)_{0.5}$ are similar. Furthermore, hydrogen uptake is similar as well. Consequently, the cross section of $H_2$ in these systems is similar, including a negligible absorption for $H_2$ in the 2a sites. In contrast, $Zn_2(bpdc)_2(bpee)$ shows a large integrated area and little hydrogen uptake, namely, ∼30% of that of $Zn(bdc)(ted)_{0.5}$. The absorption intensity per $H_2$ molecule is almost an order of magnitude higher than that for $H_2$ in any of the other MOFs studied here (see Figure 9). The origin of this larger cross section must therefore lie in the specifics of the interaction with the MOF. In $Zn_2(bpdc)_2(bpee)$, calculations indicate that $H_2$ should reside in a site where $H_2$ interacts with several benzene rings without a clear center of symmetry, as illustrated in Figure 14. Thus, the IR intensity may be a sensitive measure of the number of ligands that interact with the $H_2$ molecule. The fact that the IR intensity depends sensitively on the site is illustrated by the results for $Zn(bdc)(ted)_{0.5}$. In this MOF, the face center site was calculated to have a negligible contribution to the IR spectrum compared to the corner sites due to its more symmetrical position. Here the normalized absorption intensity in a different system ($Zn_2(bpdc)_2(bpee)$ in Table 2) further shows that the interaction with the organic ligand with the most benzene rings leads to a much larger dipole moment. As shown in Figure 14, the adsorption site is very asymmetric and there is probably a relatively large dipole moment for *all* the orientations around the equilibrium position. In contrast, the two H atoms of the adsorbed dihydrogen at the corner sites in $Zn(bdc)(ted)_{0.5}$ experience a more symmetric potential except when the bond is somewhat aligned along

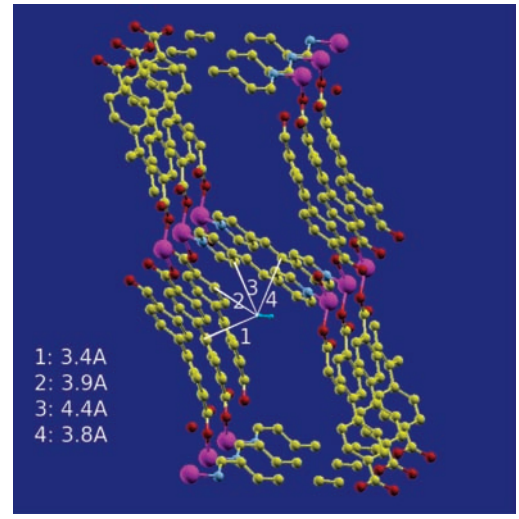


***Figure 14.*** Adsorption sites in $Zn_2(bpdc)_2(bpee)$. The interaction lines between one of the H atoms and carbon atoms in four different ligands are illustrated.

the body diagonal. Since the intensity reflects the temporal and spatial average behavior of the adsorbed $H_2$, a larger dipole and correspondingly higher IR intensity are expected for $H_2$ in $Zn_2(bpdc)_2(bpee)$. Also, as discussed before, the face center sites in $Zn(bdc)(ted)_{0.5}$ are almost inactive in IR, which will lead to a reduction of ∼50% in the overall normalized IR intensity, considering that the binding energies at those sites are slightly lower. Moreover, the more delocalized $\pi$-electrons in the double benzene rings in $Zn_2(bpdc)_2(bpee)$ are more easily perturbed by the adsorbed $H_2$ than those in the single benzene ring in $Zn(bdc)(ted)_{0.5}$. The permanent quadrupole of $H_2$ will therefore induce a larger dipole on the framework atoms of $Zn_2(bpdc)_2(bpee)$. As a result of these three factors, the IR intensity for the $Zn_2(bpdc)_2(bpee)$ system is an order of magnitude higher. The calculations, unfortunately, are not able to give the dipole moment in $Zn(bpdc)_2(bpee)$ since one of the cell parameters is only about 7 Å (leading to intercell interactions) and a larger supercell is needed to get an accurate estimation of the dipole.

## 5. Conclusions

This work highlights the effects of $H_2$ interaction within MOF structures and the relevance of combined IR absorption measurements and vdW-DF calculations.

First, the ligands are not static but respond to the incorporation of guest molecules. The response increases with the polarizability of the guest molecules, i.e., is sensitive to dispersion forces. This effect creates a challenge to carry out IR absorption experiments and can lead to possible misassignments. The use of $D_2$ as the reference is critical to study $H_2$ incorporation, although not all IR intensity changes of the MOF ligands can always be eliminated.

Second, the chemical nature of the ligands greatly affects their interaction with $H_2$ molecules. Although this interaction may affect the binding energy of $H_2$, there is no clear correlation. Binding energies correlate more closely with the size of the pores. In contrast, the nature of the interaction directly controls the H−H stretch frequency. The study of MOFs with different organic ligands and pore structures

shows that having organic ligands with $\pi$-electrons such as benzene rings increases the H−H frequency shift more than for ligands without $\pi$-electrons. For most MOFs with saturated metal centers, such as M(bdc)(ted)$_{0.5}$ systems (M = Zn, Ni, Cu) that have 3-D pore structures, there is no dependence of hydrogen adsorption on the metal center as illustrated by IR measurements and confirmed by vdW-DF calculations.

Third, for MOFs having 1-D pore structures, such as M−Fa systems (M = Ni, Mn, Co), there is a weak indirect dependence of the $H_2$ interaction on the metal center. This interaction originates from a change in pore size rather than a direct interaction with the metal centers. In these smaller micropores with restricted "necks", frustrated translational states can be observed, located $\sim\pm100$ cm$^{-1}$ away from the fundamental hydrogen IR mode, due to increased anharmonic interactions between translational and vibrational modes.

Finally, the integrated intensity of the $H_2$ stretch modes is a sensitive measure of the number and symmetry of the sites and the local interactions between $H_2$ and the organic ligands. Highly symmetric sites lead to substantially reduced dynamic dipoles, while asymmetric sites with multiple interaction points between $H_2$ and the ligands produce enhanced cross sections.

With the knowledge of perturbations induced on the MOF by guest molecules and the nature of the interactions, it is now possible and important to explore additional $H_2-H_2$ interactions that arise at higher loadings (i.e., lower temperatures) and stronger $H_2$−metal interactions that can be achieved in MOFs with unsaturated metal centers.

**Acknowledgment.** This work is supported in full by the Department of Energy (DOE Grant No. DE-FG02-08ER46491).

**Supporting Information Available:** Crystal structures of $M_3(HCOO)_6$ and M(bdc)(ted)$_{0.5}$ systems, high-pressure IR data analysis, room-temperature high-pressure isotherm measurement of Zn(bdc)(ted)$_{0.5}$, and infrared spectra of $M_3(HCOO)_6$ systems showing the effect of electronegativity and the unit cell dimension on the IR combination bands. This material is available free of charge via the Internet at http://pubs.acs.org.

JA908817N